

# New Methodology to Evaluate the Performance of Ring Resonators Using Optical Low-Coherence Reflectometry

Y. Gottesman, E. V. K. Rao, and D. G. Rabus

**Abstract**—This paper describes the efficient implementation of optical low-coherence reflectometry (OLCR) measurements to evaluate the performance of InP-based high-index contrast ring resonators. Using examples of racetrack ring resonators, this paper shows here for the first time that all characteristic parameters relevant to resonator design (coupling coefficient  $\kappa$ , propagation losses  $\alpha$ , and optical cavity length  $L$ ), and ultimately its performance, can be extracted in a straightforward manner. This is accomplished by introducing a new methodology that implicates OLCR measurements in *transmission and also reflection modes* as an alternative approach, in comparison with conventional spectral analysis, to extract resonator design parameters.

**Index Terms**—Filter analysis, integrated optics, interferograms and reflectograms, optical low-coherence reflectometry (OLCR), racetrack-shaped resonators, ring design parameters, ring resonators, transmission and reflection modes, wavelength-division multiplexing (WDM).

## I. INTRODUCTION

SEMICONDUCTOR-BASED high-index contrasted microring resonators undoubtedly offer highly promising and elegant solutions to accomplish a large variety of optical functions crucial to dense-wavelength-division-multiplexing (DWDM) networks. A few examples are the signal routing, wavelength filtering, and more specifically the add/drop function of a wavelength [1]–[3]. In all these applications, the most sought characteristics of a ring resonator are its intrinsic quality or the  $Q$  factor, its finesse  $F$ , and the free spectral range (FSR). Obviously, these characteristics are critically dependent on the ring-design-related parameters such as propagation loss ( $\alpha$ ), coupling coefficient ( $\kappa$ ), and the optical cavity length ( $L$ ).

Conventionally, the performance of ring resonators is evaluated in the wavelength space (or  $\lambda$  space) by recording the

filter response under very high spectral resolution often in a limited domain. The ring-design-related parameters are subsequently extracted from a best fit between computed and measured spectral responses [4]–[6]. This task, however, becomes tedious and time consuming for filters with high  $Q$  and high  $F$  values, since they impose the use of a high-resolution spectrometer and a finely tunable laser source in addition to remarkable experiment stability. In addition, such high resolutions are not easily accessible to an everyday optical spectrum analyzer (OSA). Furthermore, in the early stages of resonator conception and fabrication, the spectral analysis of filters can be delicate due to the presence of unwanted reflections in the ring and/or in the surrounding optical circuit.

In this context, this paper proposes and demonstrates an alternative approach that implies the use of optical low-coherence reflectometry (OLCR) technique to extract the ring resonator design parameters almost in a straightforward way by analyzing devices both with and without antireflective (AR) coatings.

This paper is partitioned into different sections, each containing specific information. Based on the analogy between ring resonators and conventional Fabry–Pérot (FP) filters, Section II first develops a set of arguments that confirm undeniably the suitability of low-coherence reflectometry (which is known to explore filter information in the time or space domain) to analyze ring resonators. As these devices operate exclusively in throughput conditions, the remainder of this section describes a novel measurement procedure using OLCR in transmission mode to facilitate the recording of interferograms. Section III is devoted to the newly developed methodology wherein a procedure to extract resonator design parameters from the OLCR recorded interferograms is detailed. Here, a few examples are provided of interferograms computed with  $\kappa$  and  $\alpha$  as parameters deliberately chosen in the range of most probable values. Section IV is completely assigned to the presentation of data—both measured and computed—and their exploitation to extract the ring resonator design parameters ( $\kappa$ ,  $\alpha$ , and  $L$ ). Since OLCR measurements in conventional reflection mode can also provide useful information needed for filter conception, we further included such data in this section together with a specially adapted procedure to extract ring design parameters from experimental reflectograms. Finally, the principal features of this work, namely, the efficient implication of OLCR measurements to analyze high-index contrast ring resonators on InP are summarized in Section V.

Manuscript received October 28, 2003; revised March 24, 2004. This work has been supported by the Région Ile de France, SESAME Project 1377, and by the Conseil Générale de l'Essone.

Y. Gottesman was with the Laboratoire de Photonique et de Nanostructures (LPN), Centre National de la Recherche Scientifique (CNRS), Marcoussis 91460, France. He is now with the Institut National des Télécommunications, Evry 91011, France.

E. V. K. Rao is with the Laboratoire de Photonique et de Nanostructures (LPN), Centre National de la Recherche Scientifique (CNRS), Marcoussis 91460, France.

D. G. Rabus was with the Heinrich–Hertz–Institut fuer Nachrichtentechnik, Berlin 10587, Germany. He is now with Forschungszentrum Karlsruhe GmbH, Institut für Mikrostrukturtechnik, Karlsruhe 76021, Germany.

Digital Object Identifier 10.1109/JLT.2004.829216

## II. FP AND RING RESONATOR FILTER RESPONSES AS MEASURED BY OLCR

In contrast to a conventional FP cavity filter, the reflecting mirrors in a ring resonator are substituted by a coupler of coupling coefficient  $\kappa$ , and the feedback is derived from multiple round trips in the ring cavity. In addition, high values of  $Q$  factors in ring resonators are easily achieved when the propagation losses ( $\alpha$ ) in the ring are kept to a minimum. As the characteristics of a filter are essentially defined by *multiple interference*, one can further project that all relevant information specific to its performance can also be extracted by investigating its impulse response  $h(t)$  in the time (space) domain. This information, as detailed in [7] and [8], is implicitly recorded in time domain using OLCR. Such measurement performed by OLCR *in its conventional reflection mode* can be mathematically expressed as [9], [10]

$$\Re(\tau) = \left| \int \hat{r}(\nu) S(\nu) e^{i2\pi\nu\tau} d\nu \right| \quad (1)$$

$$= \left| \int \hat{r}(\nu) e^{i2\pi\nu\tau} d\nu * \int S(\nu) e^{i2\pi\nu\tau} d\nu \right| \quad (2)$$

where  $\tau$  represents the time delay between the two arms,  $\nu$  the optical frequency,  $\hat{r}(\nu)$  the complex reflectivity of the device under test and  $S(\nu)$  the probe spectral distribution, and  $*$  the convolution product.

Here,  $\Re$  represents the impulse response from the device under test (DUT) which is convoluted with a source term that limits the measurement (spatial) resolution.

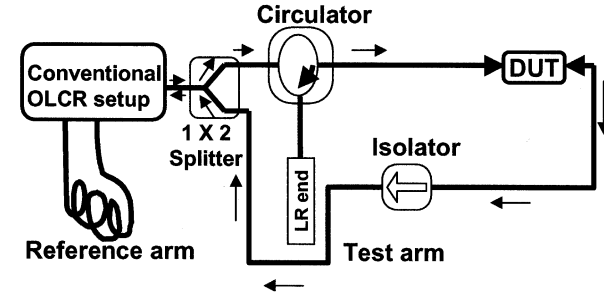
Let us now consider the reflection response of a conventional FP filter, which can be expressed as

$$\begin{aligned} \hat{r}(\nu) &= \frac{r - e^{i4\pi n\nu L/C} r^3 + t^2 r \cdot e^{i4\pi n\nu L/C}}{1 - e^{i4\pi n\nu L/C} r^2} \\ &= r + t^2 r \cdot e^{i4\pi n\nu L/C} \sum_{k=0}^{\infty} \left( r^2 e^{i4\pi n\nu L/C} \right)^k \end{aligned} \quad (3)$$

where  $r$  and  $t$  represent the mirrors reflectivity and transmission, respectively,  $L$  is the length of the physical cavity,  $C$  is the speed of light, and  $n$  is the refractive index.

A rapid examination of the second term in (3) reveals that its Fourier transform contains evenly spaced manifold Dirac-type distributions. This means the reflectogram measured by OLCR also depicts several evenly spaced peaks whose separation precisely corresponds to the optical length of the FP cavity. The first peak precisely locates the reflection at the entrance mirror, while the successive ones correspond to reflections at the exit mirror after multiple round trips of probe light ultimately collected at the entrance end (reflection mode). Consequently, the drop in reflection amplitudes between successive peaks (i.e.,  $r^2 e^{-2\alpha L}$ ) corresponds to the global loss experienced in a round trip in the cavity. This means that the two parameters (loss in a round trip and optical length of the cavity) extracted from a reflectogram are indeed self-sufficient to qualify the FP filter response. In other words, a reflectogram can also provide relevant information on the relative power of reflections and the time delay associated with each interference order contributing to ring resonator (filter) construction.

### (a) A sketch of OLCR setup in transmission mode



### (b) A simplified sketch of a ring resonator

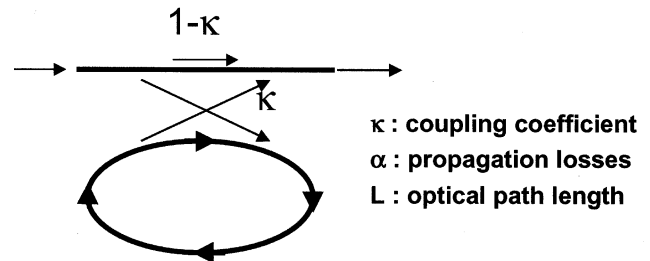


Fig. 1. Schematic representation of the upgraded OLCR setup proposed to analyze racetrack-type resonators in transmission mode. (a) Sketch of the proposed upgraded experimental setup to record interferograms. “LR” in the drawing corresponds to a low reflection end employed for reference. (b) Sketch of a racetrack resonator depicting separate input and output ports considered for transmission measurements.

The OLCR measurements traditionally performed in reflection mode exclusively describe the characteristics of a specified port into which the probe light is injected. On the other hand, the ring resonators (as in the case of add/drop devices) possess different input and output ports which must be explored separately to qualify their performance. This is accomplished by upgrading the existing equipment whose principle features [Fig. 1(a)], together with a sketch of a racetrack resonator [Fig. 1(b)], are schematically shown in Fig. 1. As seen in Fig. 1(a), the test arm contains a  $1 \times 2$  power splitter together with a circulator in one branch and an isolator in the second. Here, the prime objective is to record interference (interferograms) occurring between the probe light transmitted through the DUT and the one reflected by the mirror in the reference arm. Hence, the probe light in this configuration propagates in one way and only in one branch, which subsequently is collected at a chosen output port using a second lensed single-mode fiber (SMF). Such a measurement using this setup can now be described mathematically as

$$\Re_{l,m}(\tau) = \int \hat{h}_{l,m}(\nu) S(\nu) e^{i2\pi\nu\tau} d\nu = h_{l,m}(\tau) * \int S(\nu) e^{i2\pi\nu\tau} d\nu \quad (4)$$

where  $\hat{h}_{l,m}$  (respectively,  $l$  and  $m$ ) represents the resonator transfer function from port  $l$  to port  $m$ .

As in conventional OLCR measurements in reflection mode, the length of the reference arm in these experiments is so adjusted as to correspond to the first observed intense peak to the balanced position when DUT is introduced into the loop. In a word, these measurements are so designed as to record the interference (or interferograms) between the probe light directly

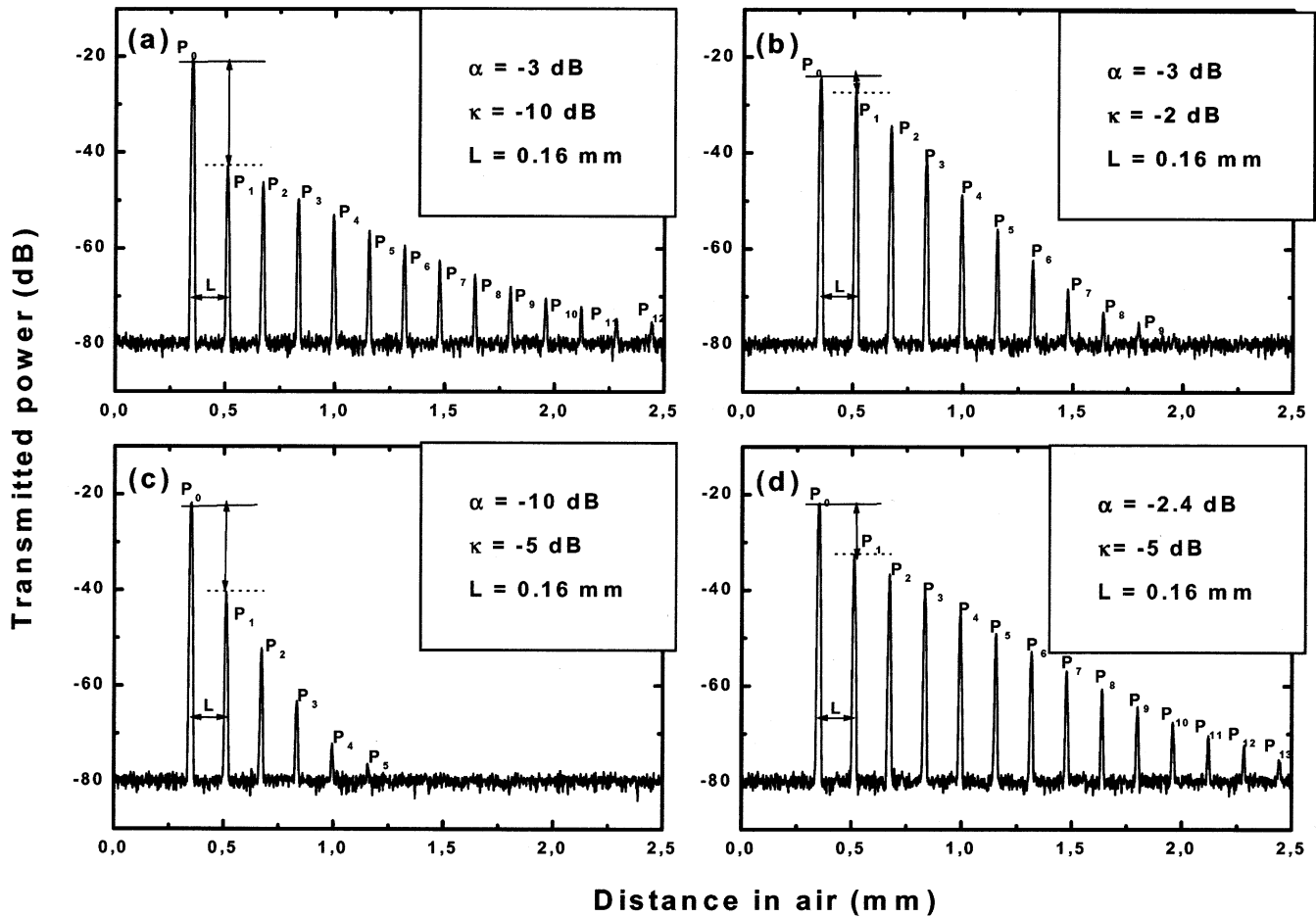


Fig. 2. Computed interferograms illustrating the high sensitivity of OLCR transmission data (transmitted power in decibels) on the ring design parameters ( $\alpha$ ,  $\kappa$  and  $L$ ). The computations are carried out using (6) in which the most probable values of  $\alpha$  and  $\kappa$  are injected for a fixed length of the ring resonator optical cavity length ( $L$ , see text for definition). The marked differences in the peak amplitudes of  $P_0$  and  $P_1$  as well as the changes in the slope of the peak amplitudes beyond  $P_1$  are noteworthy. (a)  $\alpha = -3$  dB and  $\kappa = -10$  dB. (b)  $\alpha = -3$  dB and  $\kappa = -2$  dB. (c)  $\alpha = -10$  dB and  $\kappa = -5$  dB. (d)  $\alpha = -2.4$  dB and  $\kappa = -5$  dB.

transmitted through the DUT and the one reflected from the reference mirror.

### III. EXTRACTION OF RING DESIGN PARAMETERS: PROPOSED METHODOLOGY

By considering the basic case of a racetrack-shaped ring resonator with single input and output ports [shown in Fig. 1(b)], we describe in the following paragraphs a method to extract ring parameters ( $\kappa$ ,  $\alpha$ , and  $L$ ) from the recorded interferograms. Recently, a mathematical treatment of such a device has been proposed by Yariv [11], who arrived at a simple expression that describes transmission from port 1 to port 2 ( $h_{1,2}$ ) as

$$\hat{h}_{1,2}(\nu) = \frac{-\alpha + te^{-i\theta}}{-\alpha t^* + e^{-i\theta}}. \quad (5)$$

Here,  $\alpha$  and  $t$  ( $t \cdot t^* = 1 - \kappa$ ) correspond to losses in the ring and the coupler transmission, and  $\theta$  is a dimensionless parameter equal to  $2\pi \mathbf{n} \cdot \mathbf{L} / \lambda$ , where  $\mathbf{n}$  stands for index of refraction,  $\lambda$  is the wavelength, and  $\mathbf{L}$  is the optical length of the ring cavity.

Interestingly, a close examination of (5) suggests that the transmission behavior of the racetrack resonator is described in

a manner quite analogous to that of an FP filter in reflection mode [see (3)]. In particular, (5) can be rewritten as

$$\hat{h}_{1,2}(\nu) = t + \frac{(|t|^2 - 1)}{t^*} \cdot \sum_{n=1}^{+\infty} (\alpha \cdot t^* \cdot e^{i\theta})^n. \quad (6)$$

From (6), it is now evident that the filter-related information in time domain is composed of evenly spaced localized peaks (representing transmitted power) as can be witnessed from the computed interferograms shown in Fig. 2 [see Fig. 2(a) to (d)]. These are computed using (6) and injecting ring parameters deliberately chosen in the range of most probable values [given in insets of Fig. 2(a) to (d)]. In all of these cases, the length of the ring optical cavity  $L$  is maintained at a fixed value of  $320 \mu\text{m}$ .

Turning now to Fig. 2, one can easily witness that the power in each order contributing to filter construction and also the time delay can almost be directly read from any interferogram. In other words, the interpretation of any interferogram turns out to be quite straightforward as is follows. The first peak ( $P_0$ ) corresponds to the light that traveled directly without propagating in the racetrack resonator. The second peak ( $P_1$ ), on other hand, corresponds to the light that propagated once around the ring, while the third peak ( $P_2$ ) corresponds to the light that traveled twice in the ring prior to escaping through port 2, and so on for

all other peaks of the  $P$  series. The absolute power associated to each peak deduced from (6) can be expressed as

$$\begin{cases} P_0 = \mu \cdot (1 - \kappa) P_{\text{in}} \\ P_j = \mu \cdot \kappa^2 \alpha^j (1 - \kappa)^{j-1} P_{\text{in}} \end{cases} \quad (7)$$

with  $j > 0$ ,  $\alpha$  the ring round-trip transmission,  $P_{\text{in}}$  the optical power injected, and  $\kappa = 1 - t \cdot t^*$ . Here,  $\mu$  takes into account the propagation losses experienced in the straight guide (SG) [see Fig. 1(b)].

Focusing now on the relative powers  $P_1/P_2$ , and  $P_2/P_3$ , parameters  $\kappa$  and the global propagation losses  $\alpha$  in a trip around the ring can be extracted by solving the previous set of equations (of (7)). The other parameter  $L$  namely, the optical length of the ring cavity, can be extracted from the separation between two successive peaks in the interferogram. Unlike the case of the FP filters where light propagates back and forth in the cavity, the light propagates in only one way in the ring filter. Consequently, its optical path length is twice the separation between two successive peaks [i.e., twice the value of  $160 \mu\text{m}$  indicated in Fig. 2(a)].

It is thus clear that there are three characteristic features of an interferogram recorded in transmission mode, as follows:

- 1) the difference in the amplitudes of the first two peaks— $P_0$ , representing the light directly exiting at port 2, and  $P_1$  exiting after a single passage in the resonator;
- 2) the continuously decreasing peak (power) amplitudes from  $P_1$  onwards;
- 3) a constant separation between successive peaks.

Following the proposed methodology, the design parameters can be extracted in a straightforward manner by solving the set of relations given in (7) after injecting the measured peak amplitudes taken from the experimental interferograms. We must remark here that the precision on the determination of ring parameters is only dependent on the precision to which the peak amplitudes are measured experimentally.

A strong support in favor of the proposed methodology clearly comes from the high sensitivity of interferograms to the  $\kappa$  and  $\alpha$  values. Indeed, comparing Fig. 2(a) and (b), one can notice that the higher the  $\kappa$  value, the larger is the difference between the amplitudes of peaks  $P_0$  and  $P_1$  and also the smaller is the value of peak amplitude slope from  $P_1$  onwards. Similarly, from Fig. 2(c) and (d), one can notice that the higher the  $\alpha$  value, the larger is the slope beyond  $P_1$  and also the difference in peak amplitudes between  $P_0$  and  $P_1$ . In addition, the proposed methodology has also been unambiguously validated from a direct comparison of the  $\kappa$  and  $\alpha$  values extracted from the interferograms of Fig. 2 and those employed for computing. Accordingly, this procedure has been applied in the next section to extract the ring resonator parameters from experimental interferograms recorded in transmission mode.

#### IV. RESULTS AND DISCUSSION

As mentioned previously, two families of racetrack-shaped resonator devices on InP have been investigated during this study. The details of their fabrication such as the structure of the constituent layers and the technology employed can be found in [12] and [13]. These devices contained equal bent portions of

$\sim 200\text{-}\mu\text{m}$  radius, and the power transfer between straight and ring sections is accomplished either through evanescent mode coupling or the use of a multimode interference coupler. Of the three devices investigated, only one did not contain the AR coatings at the facets. The OLCR apparatus employed here is a Michelson interferometer equipped with a Gaussian-shaped broad-band low-coherent source: a full-width at half-maximum (FWHM)  $\sim 55 \text{ nm}@1.55 \mu\text{m}$ . The device to be tested is placed in one of the interferometer arms (test arm), while the second contained a movable reference mirror. The interference signal is recorded by a detector designed to detect the fringe envelop [7].

##### A. Devices With AR Coatings in Transmission Mode

The interferograms shown in Figs. 3 and 4 represent the transmission data recorded on the two AR-coated racetrack devices using the upgraded experimental setup described previously in Section II. Interestingly, both these interferograms, like the computed ones (of Fig. 2), also depict all the three characteristic features discussed previously. Now, by simply applying the methodology detailed in Section III and solving relations given in (7), the following resonator parameters are derived from the experimental data:  $-3.8$  and  $-1.4$  dB from Fig. 3 and  $-1.7$  and  $-2.8$  dB from Fig. 4, respectively, for  $\kappa$  and  $\alpha$ . In addition, as observed from the equal separation of successive peaks in each interferogram, both devices exhibited the same optical length  $L$  equal to twice the value of  $\sim 3086 \mu\text{m}$ . These results further necessitate the following comments. First, the extraction of resonator parameters here is greatly facilitated by the detection of a *single group of peaks* (i.e., the  $P$  series) in the experimental interferograms. This is indeed a consequence of the presence of AR coatings at device facets. Second, as can be expected, the amplitude difference of  $P_0$  and  $P_1$  peaks is closely dependent on the  $\kappa$  value. Finally and most important, the ring design parameters extracted from the proposed methodology are quite close to the values deduced from conventional spectral analysis [13].

##### B. Device Without AR Coatings in Transmission Mode

Unlike in the case of AR-coated devices, the extraction of design parameters from the interferograms of devices without AR coatings can be slightly more complex due to the contribution of supplementary reflections at the facets. Such an example recorded on a device with no AR coatings is shown in Fig. 5(a). Here, one can easily distinguish the presence of a second group of peaks, signaling the fact that the transmitted light carries *combined* temporal information of two different filters: the ring resonator and the FP filter constituted by the SG [see Fig. 1(b)]. This can be easily assured of the fact that the distance separating the first peak of each group ( $P_0$  for group 1 and  $R_0$  for group 2) is precisely equal to the optical path length of the SG. Thus, as long as there is little or no overlapping between the two groups of peaks (i.e., the  $P$  and  $R$  series), the ring parameters can be extracted by simply applying the previously described methodology. This is accomplished by considering only the peaks of  $P$  series in Fig. 5(a) to find values of  $-4.6$  dB for  $\alpha$ ,  $-5$  dB for  $\kappa$ , and  $1800 \mu\text{m}$  for  $L$ . To confirm the validity of these parameters, we further carried out the computations to

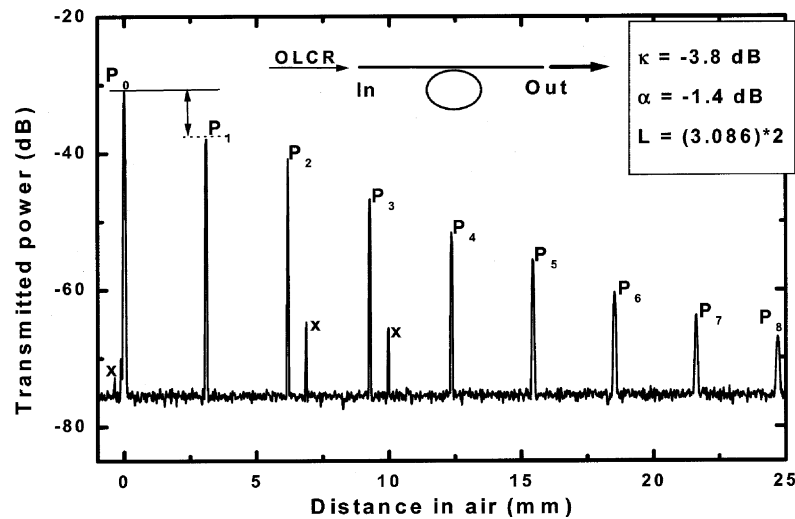


Fig. 3. OLCR-recorded interferogram (in transmission mode, see the inset drawing) belonging to a sample containing AR coatings at the device facets. The marked amplitude difference between  $P_0$  and  $P_1$  peaks and a nearly linear downward slope of peak amplitudes beyond  $P_1$  are worth noting. The ring design parameters extracted from the proposed methodology are given in the upper right-hand corner of the figure. (The peaks labeled “x” are of no concern here as they are identified to originate in the connecting fibers.)

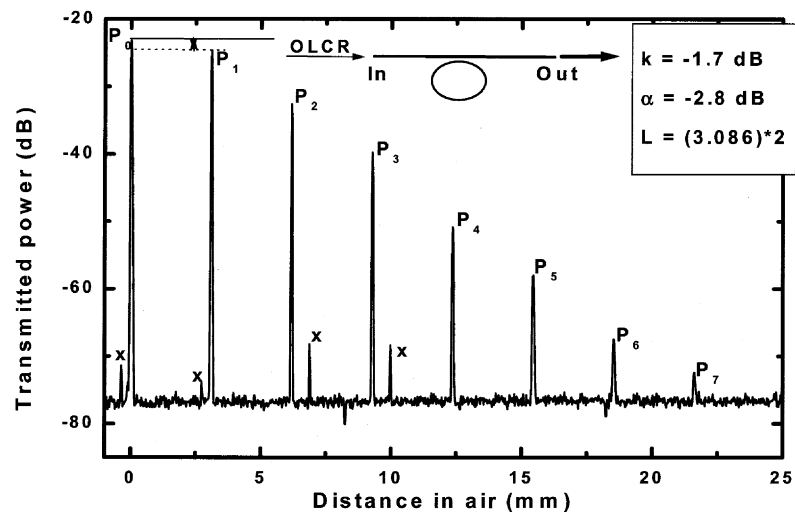


Fig. 4. OLCR recorded interferogram (in transmission mode, see the inset drawing) belonging to a second sample also containing AR coatings at the device facets. The significant decrease in the amplitude difference between  $P_0$  and  $P_1$  peaks as compared with data of Fig. 3 is worth noting (see text for details). The ring design parameters extracted by applying the methodology can be seen in the upper right-hand corner of the figure. (The peaks labeled “x” are of no concern for reasons described previously.)

find an interferogram that would contain the combined information from the two filters. These are performed by injecting in calculations the ring parameters ( $\alpha = -4.6 \text{ dB}$ ,  $\kappa = -5 \text{ dB}$ , and  $L = 1800 \mu\text{m}$ ) extracted from Fig. 5(a) and then introducing additional **reflections** at the end facets of the SG (FP resonator). More precisely, the latter reflections are included by employing transfer matrix (TM) formalism [14] and following a mathematical treatment [15] that permitted the deduction of a global transfer matrix describing the transmission across the whole system (air/SG interface, SG, ring, SG, and SG/air interface). The resulting interferogram shown in Fig. 5(b) is found to be in close agreement with the one measured experimentally [to be compared with Fig. 5(a)]. This fact clearly necessitates the following interesting remarks. First, the information carried by the first group of peaks ( $P$  series) is left unchanged despite the introduction of reflections at the SG end facets. Second, the

TM treatment applied here is adequate to include reflections. Finally, the whole methodology proposed to extract ring design parameters from experimental interferograms is indeed valid for devices both with and without AR coatings.

### C. Device Without AR Coatings in Reflection Mode

The OLCR measurements in conventional reflection mode are in general highly useful during the early stages of device conception, design, and fabrication. Such measurements on ring resonators should permit the detection and localization of undesired reflections within the device (originating from the curved portions, transition region between the curved and straight portions, even the defects induced during processing, etc.) and further help to provide a rapid feedback of design parameters in the early stages of ring fabrication. To explore precisely the latter as-

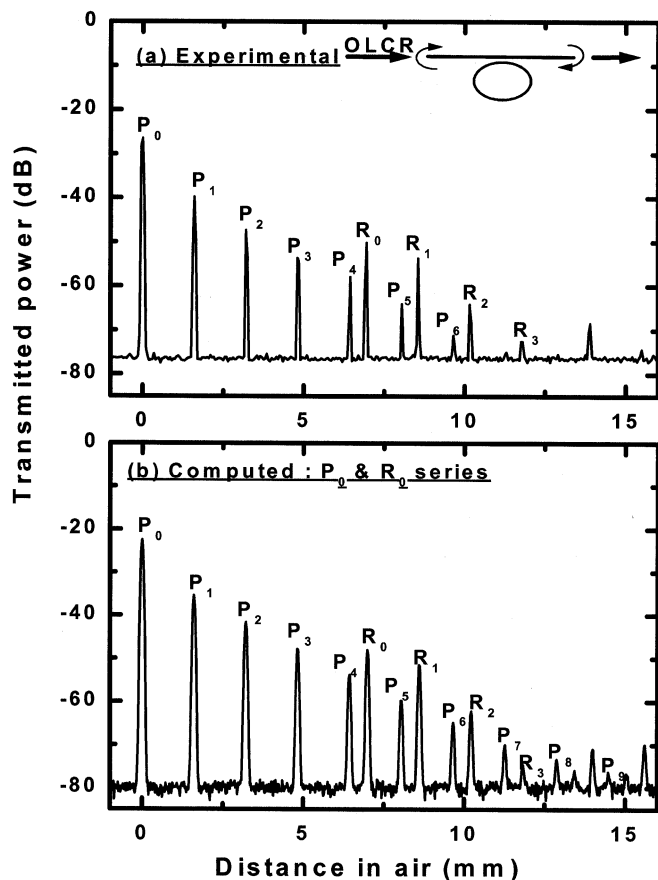


Fig. 5. Comparison of experimental and computed interferograms belonging to a sample with no AR coatings at the device facets. (a) OLCR measured interferogram in transmission mode (see the inset drawing where the curved arrows represent reflections at facets) depicting an additional group of peaks (the  $R$  series, in addition to the  $P$  series) whose presence is a result of reflections at device facets. (b) Interferogram computed by including reflections at facets using transfer matrix formalism (see text for details). The close correspondence as to the presence of two series of peaks (the  $P$  and the  $R$  series) depicting the combined features of two filters (ring and FP) clearly validate the parameter extraction procedure.

pect, we analyzed a device with no AR coatings whose results are detailed in the following paragraphs.

The reflectogram shown in Fig. 6(a) belongs to a device quite similar to those previously studied but with no coatings at the end facets (only cleaved). Here, the well-defined reflection peak seen at the beginning of the reflectogram unambiguously locates the reflection at the device input facet [labeled as “In” in Fig. 6(a)]. The two succeeding groups of peaks labeled as the  $S$  series (group 1) and the  $T$  series (group 2) signal, as before, the contribution of back-and-forth reflections occurring at the SG facets [refer to the discussion in relation to Fig. 5]. Other important features of this reflectogram to be noted are a regular decrease in the amplitude of peaks  $S_1$ ,  $S_2$ , and  $S_3$  (the  $S$  series) and a sudden change of this trend from peak  $S_4$  onwards.

Since the peaks belonging to the  $S$  series represent back-and-forth passage of probe light through the ring resonator, we have adapted the ring parameter extraction procedure accordingly to exploit the reflectogram of Fig. 6(a). This means the  $S$  series in time domain must be related to  $h_{1,2}(t)^*h_{2,1}(t)$ . Consequently,

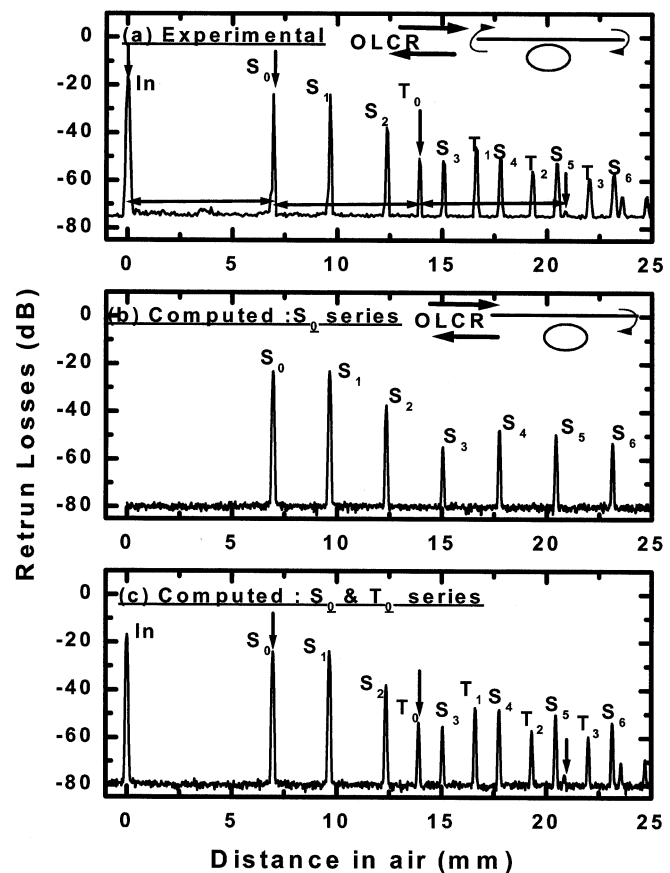


Fig. 6. Comparison of experimental and computed reflectograms belonging to a sample with no AR coatings at the device facets. (a) OLCR measured reflectogram in reflection mode (see the inset drawing where the curved arrows represent reflections at facets) depicting two groups of peaks (the  $S$  series and the  $T$  series) whose presence is related to reflections originating at device facets. The solid line with arrows on either side correspond to a round trip of the OLCR probe light in the SG and designate its optical path length. (b) Reflectogram computed by injecting the ring parameters extracted from the peaks of the  $S$  series belonging to Fig. 6(a) and further considering an identical device as in Fig. 6(a) but with AR coatings alone at the input facet (see the inset drawing). The close resemblance (in amplitude and position) between the peaks of the  $S$  series from Fig. 6(a) and (b), together with the sudden change in the slope of peak amplitudes at  $S_4$ , must be noted (see text for details). (c) Second interferogram computed by injecting ring parameters extracted from the  $S$  series of Fig. 6(a) and further considering reflections at both facets using, as before, the transfer matrix formalism. The close resemblance (peak amplitude, position, and the slope change in peak amplitudes at  $S_4$ ) between the measured [Fig. 6(a)] and computed [Fig. 6(c)] reflectograms validate the methodology described by (8) for extracting ring design parameters from OLCR data in reflection mode.

the power in the first three peaks of the  $S$  series as derived from the Fourier transform of (6) can be expressed as

$$\begin{aligned} S_0 &= \mu(1 - \kappa)^2 \\ S_1 &= \mu \cdot 4\kappa^2(1 - \kappa)\alpha^2 \\ S_2 &= \mu \cdot \kappa^2\alpha^4(2 - 3\kappa) \end{aligned} \quad (8)$$

where  $\kappa$  and  $\alpha$  have the same significance as before, while  $\mu$  represents a coefficient that takes into account the losses due to propagation and also to reflections at the SG facets.

Interestingly, one can now notice from (8) that the values of  $\kappa$  and  $\alpha$  can be directly extracted from an experimental reflectogram (i.e., with no deconvolution) by evaluating  $(S_1 \cdot S_1)/(S_0 \cdot S_2)$  and  $S_1/S_0$ .

Following this methodology, we took into consideration the first three peaks of the  $S$  series ( $S_0$ ,  $S_1$ , and  $S_2$ ) to extract the following ring design parameters:  $\kappa = -2.8$  dB,  $\alpha = -3.6$  dB and  $L = 1.5$  mm. Later on, we verified the validity of these parameters in two phases by computing two different and yet closely related reflectograms, as detailed hereafter.

In the first phase, we computed a reflectogram by injecting the previously deduced parameters in the same device but with a forbidden reflection at the device input facet (use of AR coatings to suppress multiple round trips). Interestingly, the resulting reflectogram [Fig. 6(b)] exhibits all the major evolutions of the peaks in the  $S$  series observed in the experimental reflectogram [Fig. 6(a)], although their absolute amplitudes show some small differences ( $< 3$  dB). In the second phase, to follow closely the experimental data, we further computed a second reflectogram by injecting the extracted parameters and introducing reflections at the two facets of the device (multiple round trips) through the previously described TM formalism. The close agreement between the computed [Fig. 6(c)] and measured [Fig. 6(a)] reflectograms clearly confirm the validity of the methodology described here to extract the ring design parameters when the OLCR measurements are performed in the conventional reflection mode.

## V. SUMMARY AND CONCLUSION

We have proposed in this work a new analytical procedure implying OLCR measurements as an alternative approach to conventional spectral analysis to extract the design parameters of ring resonators ( $\kappa$ ,  $\alpha$ , and  $L$ ). This procedure, in contrast to spectral domain measurements, is simple to execute and further permits a straightforward extraction of ring parameters from the experimental data. The high potential of proposed methodology is demonstrated in this study by considering the examples of racetrack resonators both with and without AR coatings at the device facets. Our choice of devices with no AR coatings (i.e., only cleaved) is mainly based on two reasons: 1) to examine the efficiency of OLCR analysis to provide a rapid feedback of ring design parameters in the early stages of device fabrication (i.e., devices that have not undergone an additional process of AR coatings) and 2) to also explore the potential of OLCR measurements in its conventional reflection mode of operation to extract ring design parameters.

Since the racetrack devices considered here generally operate under throughput conditions, the paper first proposed a new experimental setup (OLCR measurements in transmission mode) and a novel methodology to extract ring resonator design parameters from the recorded interferograms. Later on, the paper described successful treatment of the case of devices with no AR coatings in the framework of newly proposed transmission mode by incorporating reflections at facets using a transfer matrix formalism. Finally, the case of OLCR measurements in its conventional reflection mode was also considered and data was presented to demonstrate their efficiency to extract the ring design parameters, particularly useful during the early stages of their conception and fabrication. In conclusion, as in earlier reports [16]–[18], this paper demonstrates that the OLCR measurements can be fruitfully employed to extract relevant information on design optimization and processing technologies as

well as the performance evaluation of several key photonic components presently developed on InP [19].

## REFERENCES

- [1] E. A. J. Marcetili, "Bends in optical dielectric guides," *Bell. Syst. Tech. J.*, vol. 48, pp. 2103–2132, 1969.
- [2] B. E. Little, S. T. Chu, H. A. Haus, J. Foresie, and J.-P. Laine, "Microring resonator channel dropping filters," *J. Lightwave Technol.*, vol. 15, pp. 998–1005, June 1997.
- [3] Y. Carts-Powell, "Microresonators provide optical building blocks," *Laser Focus World*, pp. 18–22, July 1997.
- [4] D. Rafizadeh, J. P. Zhang, R. C. Tiberio, and S. T. Ho, "Propagation loss measurements in semiconductor microcavity ring and disc resonators," *J. Lightwave Technol.*, vol. 16, pp. 1308–1313, July 1998.
- [5] B. Vanderhaegen, D. Vanthourhout, J. De Merlier, G. Sarlet, L. Vanwassenhove, I. Moerman, P. Van Daele, R. Baets, X. J. M. Leijtens, J. W. M. Van Uffelen, and M. K. Smit, "High Q InGaAsP ring resonator filters," in *Proc. Eur. Conf. Integrated Optics (ECIO'99)*, Turin, Italy, Apr. 1999, pp. 381–384.
- [6] D. G. Rabus, M. Hamacher, U. Troppenz, and H. Heidrich, "Optical filters based on ring resonators with integrated semiconductor optical amplifiers in GaInAsP-InP," *IEEE J. Select. Topics Quantum Electron.*, vol. 8, pp. 1405–1411, Nov./Dec. 2002.
- [7] B. L. Danielson and C. D. Whittenberg, "Guided-wave reflectometry with micrometer resolution," *Appl. Opt.*, vol. 26, pp. 2836–2842, July 1987.
- [8] K. Takada, I. Yokohama, K. Chida, and J. Noda, "New measurement system for fault location in optical waveguide devices base on an interferometric technique," *Appl. Opt.*, vol. 26, pp. 1603–1605, 1987.
- [9] U. Wiedmann, P. Gallion, and G. H. Duan, "A generalized approach to optical low-coherence reflectometry including spectral filtering effects," *J. Lightwave Technol.*, vol. 16, pp. 1343–1347, July 1998.
- [10] Y. Gottesman, "Exploitation of low-coherence reflectometry to the analysis photonic components and circuits," Ph. D. dissertation, University of Aix-Marseille III, Marseille, France, 2001.
- [11] A. Yariv, "Universal relations for coupling of optical power between microresonators and dielectric waveguides," *Electron. Lett.*, vol. 36, pp. 321–322, Feb. 2000.
- [12] D. G. Rabus and M. Hamacher, "MMI-coupled ring resonators in GaInAsP-InP," *IEEE Photon. Technol. Lett.*, vol. 13, pp. 812–814, Aug. 2001.
- [13] D. G. Rabus, "Realization of optical filters using ring resonators with integrated semiconductor optical amplifiers in GaInAsP-InP," Ph.D. Electrical Engineering and Computer Science Dept., Technical Univ., Berlin, Germany, 2002.
- [14] M. Yamada, M. Leblanc, M. M. Ohn, and R. M. Measures, "Analysis of almost-periodic distributed feedback slab waveguides via a fundamental matrix approach," *Appl. Opt.*, vol. 26, pp. 3474–3478, 1987.
- [15] Y. Gottesman and E. V. K. Rao, "A simplified numerical treatment of reflections in ring resonators based on transfer matrix formalism," to be published.
- [16] Y. Gottesman, E. V. K. Rao, and B. Dagens, "A novel design proposal to minimize reflections in deep-ridge multi-mode interference couplers," *IEEE Photon. Technol. Lett.*, vol. 12, pp. 1662–1664, Dec. 2000.
- [17] Y. Gottesman, E. V. K. Rao, H. Sillard, and J. Jacquet, "Modeling of low-coherence reflectometry recorded Bragg reflectograms: Evidence to a decisive role of Bragg spectral selectivity," *J. Lightwave Technol.*, vol. 20, pp. 489–493, Mar. 2002.
- [18] E. V. K. Rao, Y. Gottesman, and J. G. Provost, "Simple method to diagnose the performance of electroabsorption modulators on InP using low-coherence reflectometry," *Appl. Phys. Lett.*, vol. 81, pp. 1552–1554, Aug. 2002.
- [19] E. V. K. Rao and Y. Gottesman, "Design, process and performance diagnosis of InP-based photonic components using low-coherence reflectometry," in *Proc. Int. Conf. Indium Phosphide and Related Materials (MIPRM'03)*, Santa Barbara, CA, May 2003, FA2-1, pp. 544–545.

**Y. Gottesman**, photograph and biography not available at the time of publication.

**E. V. K. Rao**, photograph and biography not available at the time of publication.

**D. G. Rabus**, photograph and biography not available at the time of publication.